Compact ultrahigh vacuum sample environments for x-ray nanobeam diffraction and imaging
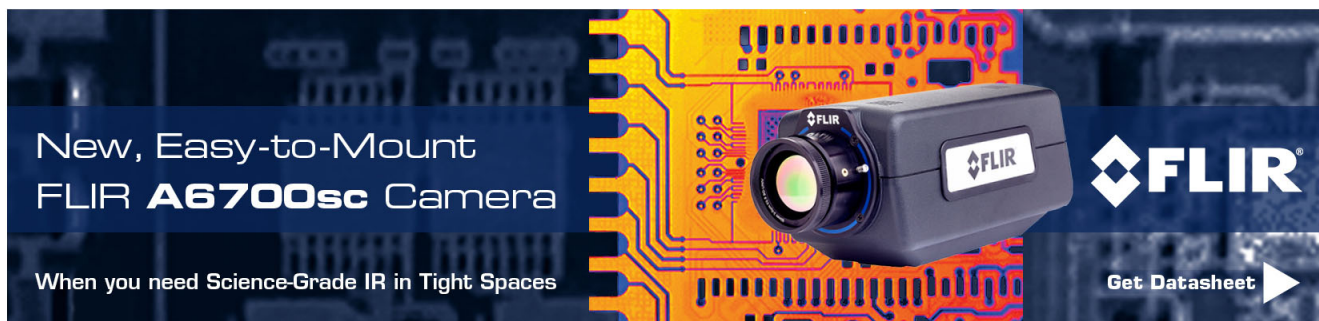
P. G. Evans, G. Chahine, R. Grifone, V. L. R. Jacques, J. W. Spalenka, and T. U. Schülli

Compact ultrahigh vacuum sample environments for x-ray nanobeam diffraction and imaging

P. G. Evans,[1,a] G. Chahine,[2] R. Grifone,[2] V. L. R. Jacques,[2,b] J. W. Spalenka,[1] and T. U. Schülli[2]

[1]*Materials Science and Engineering, University of Wisconsin-Madison, Madison, Wisconsin 53706, USA*
[2]*European Synchrotron Radiation Facility, Grenoble 38043, France*

X-ray nanobeams present the opportunity to obtain structural insight in materials with small volumes or nanoscale heterogeneity. The effective spatial resolution of the information derived from nanobeam techniques depends on the stability and precision with which the relative position of the x-ray optics and sample can be controlled. Nanobeam techniques include diffraction, imaging, and coherent scattering, with applications throughout materials science and condensed matter physics. Sample positioning is a significant mechanical challenge for x-ray instrumentation providing vacuum or controlled gas environments at elevated temperatures. Such environments often have masses that are too large for nanopositioners capable of the required positional accuracy of the order of a small fraction of the x-ray spot size. Similarly, the need to place x-ray optics as close as 1 cm to the sample places a constraint on the overall size of the sample environment. We illustrate a solution to the mechanical challenge in which compact ion-pumped ultrahigh vacuum chambers with masses of 1–2 kg are integrated with nanopositioners. The overall size of the environment is sufficiently small to allow their use with zone-plate focusing optics. We describe the design of sample environments for elevated-temperature nanobeam diffraction experiments demonstrate *in situ* diffraction, reflectivity, and scanning nanobeam imaging of the ripening of Au crystallites on Si substrates. © 2013 AIP Publishing LLC. [http://dx.doi.org/10.1063/1.4829629]

I. INTRODUCTION

Recent developments in focusing x-rays to nanometer-scale focal spot sizes and in interpreting coherent scattering from nanoscale objects promise to provide tremendous insight into the atomic-to-mesoscale structure of emerging materials.[1,2] Nanobeam techniques, however, have largely been applied in sample conditions far from the regimes of pressure and temperature at which it would be most useful to understand the properties of materials. In part this is because sample environments have been incompatible both with nanopositioning instruments and with the small 0.5–2 cm working distances of nanofocusing optics. The result has been that x-ray scattering and diffraction studies have been limited to studies at high-temperature or challenging environments with comparatively large micron-to-millimeter scale large x-ray beams[3,4] or to studies with x-ray nanobeams under ambient or near-ambient conditions.[5–7] A few cases have demonstrated that the integration of nanobeams with more complex environments is indeed possible, e.g., in the use of x-ray zone plate optics with continuous-flow cryostats,[8] or by mounting the focusing optics within the vacuum environment,[9] but at the cost of reduced experimental versatility.

Removing the limitations imposed by the lack of sample environments compatible with nanobeam techniques will greatly extend the range of *in situ* x-ray nanobeam studies. Nanobeam techniques have the potential to contribute to enhanced understanding of nanomaterials, catalysis, and self-assembly, for which other microscopic probes are not available. X-ray nanobeam studies can provide new information about individual nanocrystals, defects, domain structures, and patterned features, as well as the evolution of these features a function of time.[1] Realizing the full potential of x-ray nanobeam technologies requires the capability to perform the entire range of x-ray nanobeam experiments while the sample is held under challenging conditions of high temperatures and controlled ambient gasses.

Two key instrumental challenges must be addressed in the design of sample environments to allow a wider range of conditions to be explored in x-ray nanobeam experiments. First, x-ray nanofocusing requires that x-ray optics must be positioned close to the sample, greatly limiting the volume available for sample environments. The x-ray optics required to focus x-rays to the 20–100 nm spot sizes presently available have numerical apertures on the order of approximately 10^{-3}–10^{-2}.[10] In addition, the final x-ray optical element before the sample in a nanobeam instrument consists of either a final mirror in systems in which the focusing optics are based on Kirkpatrick-Baez mirrors,[11] or an order-sorting aperture in systems based on zone-plate optics.[12] Similar apertures are often employed to eliminate unfocused radiation in systems employing compound refractive optics.[13] These final optical elements are typically placed at distances of 0.5–2 cm from the sample.

A second challenge arises because the location of volume probed by the x-ray beam is varied during experiments by changing the relative position of the sample and the

---

a)Electronic mail: evans@engr.wisc.edu
b)Present address: Laboratoire de Physique des Solides (CNRS-UMR 8502), Bât. 510, Université Paris-sud, 91405 Orsay cedex, France.

84, 113903-1

focusing optics. Nanodiffraction experiments require accurate control of the relative orientation of the sample with the incident beam and thus require that the beam pass through the center of rotation of the diffractometer. The alignment must be maintained in order to make accurate angular measurements and to avoid changing the position of the x-ray beam on the sample when the sample is rotated. For nanodiffraction experiments, the relative position of the optics and sample must be set by translating the sample because translating the optical elements moves the focused x-ray beam off of the center of rotation of the diffractometer. Positioners with accuracy sufficient for nanobeam experiments typically have useful payloads of on the order of 1 kg at most, and these positioners typically operate under room-temperature atmospheric pressure conditions. The challenge is to develop sample environments that are compatible with these size and positioning constraints.

We show here that nanobeam sample environments with wide temperature ranges and control over ambient conditions can resolve these challenges. We build on concepts developed for previous compact sample environments,[14, 15] and minimize both the mass of the overall structure and the stiffness of its connections to auxiliary equipment such as pumps and power supplies. We present detailed descriptions and experimental tests of ultrahigh vacuum (UHV) sample environments with low masses and compact shapes that allow them to be integrated with nanobeam diffractometers. A key conceptual aspect of these sample environments is that the pre-pumping with a turbomolecular pump is followed by complete detachment from mechanical pumps and the subsequent use of a lightweight ion pump to maintain the vacuum thereafter. The design of the sample environment and the chamber has a sufficiently low rate of outgassing so that the entire sample environment vacuum can be pumped continuously using an ion pump at the temperatures of interest. The use of an ion pump avoids rigid connections, such as vacuum bellows, that would transmit vibration and impose an additional mechanical load on the nanopositioners supporting the sample environment. The experimental test of these instruments was conducted in an *in situ* study of the evolution of the structure of a gold thin film on Si (100) during annealing.

II. NANOBEAM SAMPLE ENVIRONMENT DESIGN

We present here two sample environments in which the sample is mounted on a small resistive heater, as shown in Fig. 1. The heater (Heat Wave Labs, Inc.) has a diameter of 8 mm for which the electrical current is provided by a feed-through in the base of the instrument. This heater specially designed to work in vacuum. Its maximum operating temperature of 1200 °C requires an electrical power of approximately 30 W at that temperature. The base of the heater is mounted on a quartz tube for electrical and thermal isolation. The tube in turn is supported by a retaining ring on the interior diameter of a short vacuum nipple with CF16 ports (Kimble Physics, Inc.). The combined thermal expansion of the heater and quartz tube result in a displacement of the sample along the surface normal by 50 nm/K, which must be compensated by translating the stage when the temperature is
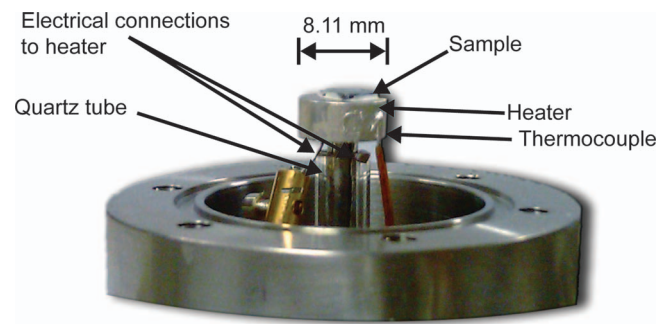

FIG. 1. Sample, electrical connections, and vacuum flange connection to the dome in the sample environment based on a Be dome x-ray window.

changed. In the temperature range of the results reported below, the temperature response to a step increase in the heater power was exponential with a thermal settling time constant of 16 min. The temperature at the heater is measured using either a Pt wire resistor (PT-111, LakeShore Cryotronics, Inc.), a thermocouple, or using a phase transition with a known temperature.

Electrical connections are provided by a CF16 electrical feed-through (MDC, Inc.) connected to the opposite end of the nipple. Access to the sample is allowed when the x-ray windows are removed. The sample can be either glued or clamped on the button heater. An important feature of the design of the heater stage is that the sample reaches a temperature range of scientific interest of several hundred °C with modest electrical power on the order of 10 W or less. The mechanical design is compact and robust in order to minimize drift in the position and orientation of the sample.

There are two strategies for building the sample vacuum environment around the sample post shown in Figure 1. The first of these uses planar Be x-ray windows, which introduce a minimum of additional material into the beam. The planar-window design allows optical access to the top of the sample via a viewport opposite the feed-through on which the sample is mounted. A second strategy uses a Be dome, which provides the maximum possible range of scattering geometries. The dome strategy, however, requires a greater thickness of Be and reduces optical access to the sample.

A. Sample environment with planar Be windows

A schematic of the sample environment based on two planar windows is shown in Figure 2(a). The vacuum chamber for the sample environment uses a stainless steel UHV cross with two CF40 flanges and four CF16 flanges (Kimball Physics, Inc.). The Be windows were mounted on the CF40 faces, with the planes of the window located at a distance of 2 cm from the center of the top of the sample heater. The sample post is mounted on one of the four CF16 flanges. An ion pump (Kernco, Inc.) is mounted on one of the remaining CF16 ports. As shown in the photo in Figure 2(b), the sample post is mounted to place the sample slightly below the center of the UHV cross to maximize the available range of scattering angles. The use of metal-seal flanges allows this system to use vacuum seals based on Cu gaskets and thus to be baked to
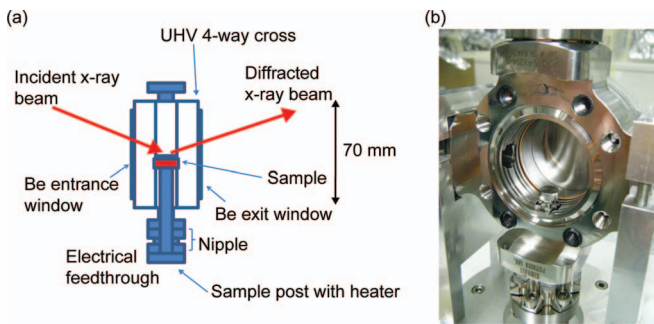
FIG. 2. (a) Diagram and (b) photograph of the x-ray nanodiffraction sample environment using planar Be windows with one window removed. The sample heater is visible just below the center of the image.

approximately 150 °C before beginning the experiment. The initial evacuation of the sample environment is performed using a turbomolecular pump connected to the chamber through a UHV-compatible gas valve. The system can also be baked while using the turbomolecular pump. When the ion pump has been started and the chamber is mounted on the x-ray diffractometer the turbomolecular pump is detached from the system. During its operation at beamline ID01 of the European Synchrotron Radiation Facility (ESRF), the sample environment with flat Be windows was mounted on a hexapod translation and tilt stage (Symetrie, Nîmes, France). This arrangement allowed minimum step sizes on the order of 50 nm, with long-term stability and reproducibility of better than 1.5 μm. Raising the temperature of the sample to 245 °C required a heater power of 2.4 W.

B. Sample environment with Be dome

The sample environment based on Be dome x-ray window is shown in Figure 3. This system uses a custom vacuum chamber in which the port for the sample post is opposite the port occupied by the 25 mm-diameter Be dome. Orthogonal ports are used for an ion pump and for the connection to the turbomolecular pump. After the turbomolecular pump is detached the chamber has a mass of 1.4 kg. The mass is sufficiently low that the chamber can be mounted directly on a three-axis piezoelectric positioning stage (Physik Instrumente, Inc.). The piezoelectric stage translates the sample with an accuracy of 10 nm over lateral distances of 200 μm and a vertical range of 100 μm. The vertical and horizontal fixtures connecting the vacuum chamber to the piezoelectric stage are rigid in order to allow this precision to be maintained as the environment and stage are rotated by the diffractometer.

The tests described below formed the vacuum seal between the Be dome and the body of the sample environment using a Viton gasket. This choice is convenient, but limited the bake-out temperature and ultimate pressure of the dome-based chamber to the 10^{-7} Torr range. The Viton seal thus allowed the chamber to reach pressures sufficiently low that the vacuum could be maintained by the ion pump. Applications demanding lower pressures would require that the Viton gasket be replaced with a metal gasket.
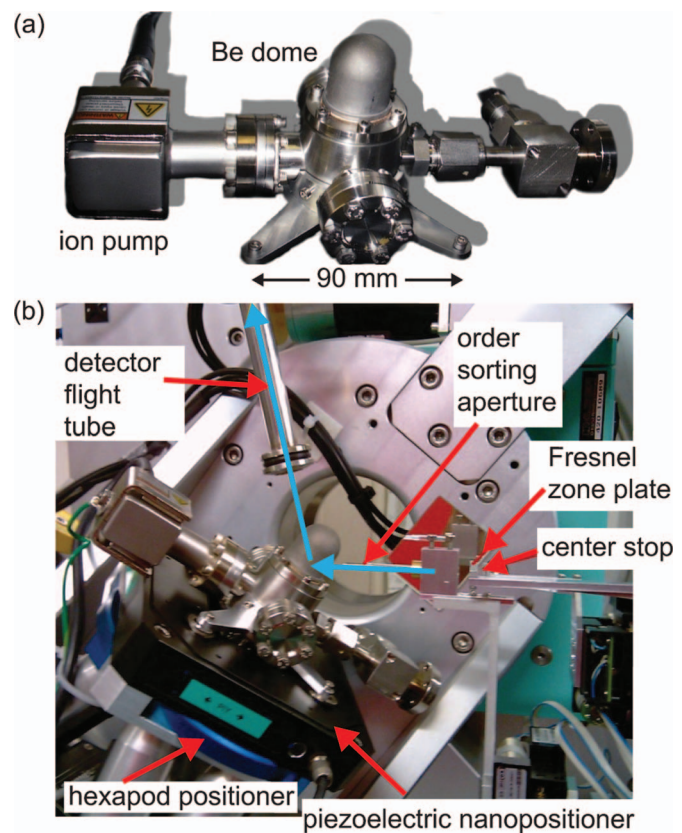

FIG. 3. (a) Sample environment using a 25-mm diameter Be dome. (b) The sample environment mounted on the three-axis piezoelectric sample stage in a Bragg diffraction geometry. The components of the Fresnel-zone-plate optics are visible near the Be dome. Arrows indicate the x-ray beam path from the source (right) to the detector (left).

III. RESULTS OF *IN SITU* X-RAY NANOBEAM EXPERIMENTS

The operation of the two sample environment was tested and compared in a series of *in situ* x-ray studies performed at the ID01 beamline of the ESRF. The two different sample environments were used to conduct *in situ* x-ray reflectivity, diffraction, and nanobeam diffraction mapping experiments. The experiments probed the evolution of the structure and morphology of Au thin films deposited on Si surfaces.

In a series of experiments with the planar Be window environment, x-rays with photon energy of 8 keV were focused to a spot size of approximately 200 nm in the vertical direction by a Fresnel zone plate (FZP). The zone plate had a diameter of 200 μm and an outermost zone width of 70 nm, giving focal length of 12.5 cm at 10 keV.[16] Unfocused radiation transmitted by the FZP is eliminated using a combination of a 60 μm center stop placed just before the FZP and an order sorting aperture with a 50 μm in diameter positioned 2.5 cm before of the sample. A second series of experiments with the system based on a Be dome used a photon energy of 10 keV. In both experiments, the scattered x-rays were detected using a two-dimensional Maxipix pixel array detector.[17] The evolution of a 2 nm Au layer on Si (111) was studied using the Be dome sample environment in a similar x-ray diffraction mapping arrangement. All experiments were performed in a

vertical scattering geometry, as illustrated in the case of the experiment with the Be dome environment in Figure 3(b).

A. *In situ* evolution of the crystallographic texture of Au/Si (001)

The sample environment based on two parallel Be windows was tested in a structural study of the evolution of the microstructure of an Au layer on Si (001) at elevated temperatures. The sample for these experiments consisted of an Au thin film with a thickness of 6 nm deposited on an Si (001) substrate. In order to prepare the Au films, the samples were cleaved from an Si (001) wafer, immersed in a 5% HF solution for 10 min, rinsed for 10 min in deionized water and then dried with a nitrogen gun. The samples were then immediately transferred to an electron beam evaporation chamber in which the Au was deposited. Individual Au/Si (001) samples with dimensions of 3×3 mm^2 were cleaved from sample and mounted on the sample heating stage using epoxy.

The room-temperature deposition of thin Au layers on Si and other substrates leads to the creation of a polycrystalline, smooth Au film.[18,19] The Au atoms have sufficient mobility, however, that even at modest elevated temperatures of 100–300 °C the Au layer transforms into a series of far larger isolated Au crystallites. The crystallites are oriented so that (111) planes are parallel to the substrate surface. The expected transformation from a relatively smooth polycrystalline layer to a series of isolated crystallites is shown schematically in Fig. 4(a).

The evolution of the structure of the Au/Si (001) film during annealing was probed using diffraction, reflectivity, and by forming images of the intensity of the Au (111) reflection as a function of the position of the x-ray beam on the sample. Diffraction patterns acquired near the Au (111) reflection during the heating to 245 °C are shown in Fig. 4(b). The lowest temperature diffraction pattern in 4(b) was acquired at 91 °C. The diffracted intensity in the 91 °C panel of Fig. 4(b) is broadly distributed across a wide range of angles in both the diffraction angle 2θ and in the out-of-plane diffraction angle χ, indicating that Au layer is initially polycrystalline before annealing. The width of the reflection in Fig. 4(b) and the lack of a preferred direction indicate that the Au layer is initially composed of small crystals with a random distribution of orientations.

The initially diffuse diffraction pattern sharpens dramatically as the sample is subsequently heated to higher temperatures. The diffraction patterns at 194, 213, 234, and 245 °C of Fig. 4(b) exhibit a progressive decrease in the broad polycrystalline Au reflection and the development of a sharp Au (111) reflection. This redistribution of the intensity at the Au (111) reflection arises from the development of a (111) texture in the Au layer. The development of the (111) texture is particularly pronounced in the diffraction pattern 245 °C in Fig. 4(b), in which a sharp isolated Au (111) Bragg reflection is apparent.

The lattice constants of the Au crystals also change during heating. A series of θ–2θ scans was assembled by analyzing diffraction patterns acquired at series of incident angles at each temperature. Measurements acquired between 92 °C and 245 °C are shown in Fig. 4(c). The Au (111) peak be-
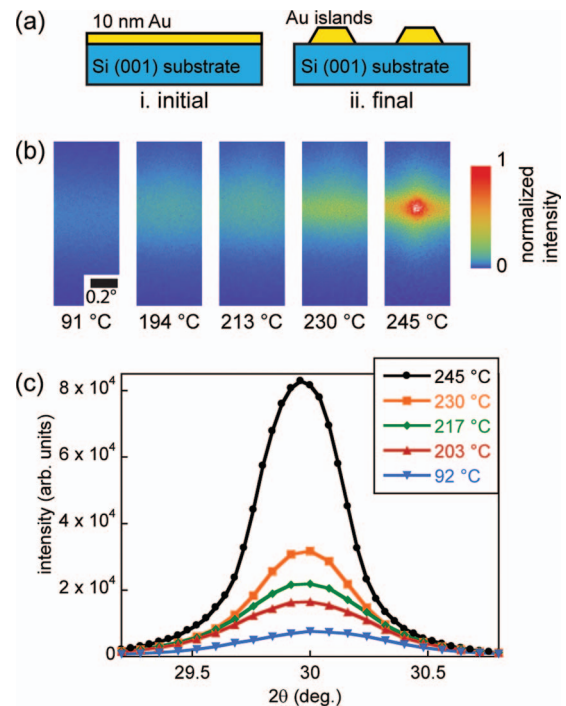

FIG. 4. (a) Initial and final structure of the Au thin film on Si (001). (b) Evolution of the Au (111) reflection from an initial diffuse powder diffraction ring at low temperature to a sharp epitaxial reflection upon annealing. Images are individual diffraction patterns collected using a two-dimensional x-ray detector. The angular scale of the diffraction patterns is given by the scale bar inset at 91 °C. (c) Evolution of the diffracted intensity in θ-2θ scans acquired during annealing.

came sharper and more intense as the temperature increases. The Au (111) shifted to lower 2θ as the structure of the Au thin film evolved. The decreased angular width and increased intensity arise from the redistribution of the intensity of the Au (111) reflection from an initially diffuse ring into a single point in reciprocal space as the sample is heated.

X-ray reflectivity profiles for the Au/Si(001) sample are shown in Fig. 5. Initially, the Au thin film is smooth and the x-ray reflectivity exhibits a series of intensity oscillations with a periodicity set by the thickness of the Au layer. The reflectivity curves acquired at lower temperatures in Fig. 5 are
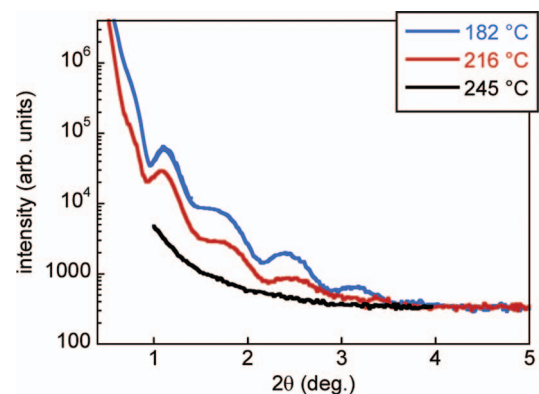

FIG. 5. (a) Evolution of the x-ray reflectivity of the Au/Si (001) system during heating. The low-temperature reflectivity signature consists of a series of fringes with a periodicity corresponding to the thickness of the Au layer. The formation of islands at higher temperatures results in the disappearance of the fringes.
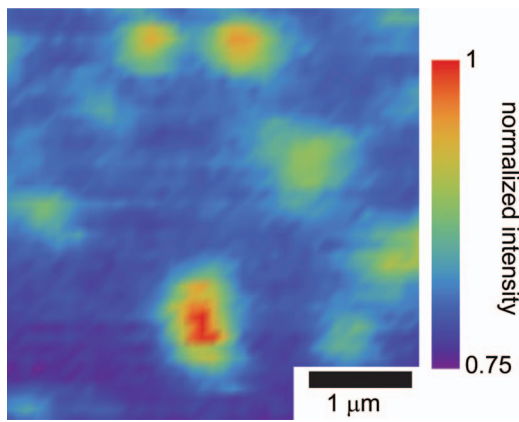
FIG. 6. X-ray diffraction nanodiffraction images of the intensity of the Au (111) reflection as a function of the location of the focused x-ray beam footprint on the sample surface, acquired at 245 °C.

accurately fit by a simulation of the reflectivity with an Au layer thickness of 6.2 nm and root-mean-square roughness of 4 Å. The oscillations persist as the sample is heated and are apparent in reflectivity measurements at temperatures as high as 216 °C. X-ray reflectivity intensity distributions acquired at 245 °C, however, do not show the periodicity associated with the Au film. The disappearance of the film-thickness oscillations in the reflectivity at high temperature is consistent with the formation of the large Au islands. The large area of exposed Si substrate provides the dominant contribution to the reflectivity signal, and there is thus only a monotonic decrease in the reflected intensity as the incident angle of the x-ray beam increases.

A map of the intensity of the Au (111) diffraction peak as a function of the position of the x-ray beam on the sample surface is shown in Fig. 6. The diffracted beam has high intensity in areas occupied by Au islands and vanishingly low intensity in areas far from islands. The initially smooth Au films thus ripen into a series of large isolated Au islands in which the (111) planes are parallel to the plane of the Si surface. At 245 °C, as shown in Fig. 6, the islands have sizes on the order of 200 nm and separations of approximately 1 μm.

B. *In situ* crystal growth from an Au/Si eutectic on Si (111)

The sample environment enclosed by the Be dome was used to study structural changes in an Au thin film on Si (111) during annealing. A 2 nm thick Au film was deposited on Si (111) under UHV conditions in a molecular beam epitaxy chamber and subsequently transferred to the nanobeam sample environment. As was the case for the Au/Si (001) thin films, heating the Au/Si(111) film results in the formation of Au islands. This process yielded islands with lateral sizes of approximately 200 nm and a strong (111) preferred orientation.

The sample environment in this case did not include a separate thermometer. The relationship between the heater power and sample temperature was calibrated by examining the melting of the Au layer using the Au (222) Bragg reflec-

tion. The temperature calibration procedure consisted of monitoring the intensity of the (222) reflection as the temperature was increased from room temperature to the Au-Si eutectic at 363 °C. Reflections from crystalline Au disappeared at the eutectic at all positions of the beam on the sample. The transition into the eutectic liquid was completed after the heater power was raised to 3.6 W, corresponding an applied voltage of 2.4 V and a current of 1.5 A, indicating that the temperature of the sample was at least 363 °C at these settings. A pressure of 5×10^{-7} Torr was reached before heating and after stabilization at the highest temperatures.

After heating the sample to Au-Si eutectic temperature, we compared the crystalline structures created by cooling the sample. First, Au islands with diameters of approximately 200 nm were created by heating the sample through the eutectic temperature and then lowering the heater power to 0.6 W. The crystalline state created by this rapid cooling was studied using diffraction mapping. The sample was then re-heated to a higher power of 2.8 W (2.0 V, 1.4 A) for 30 min. The resulting Au structure was again studied at a heater power of 0.6 W.

The Au island structures following the rapid initial cooling from the eutectic temperature and after annealing were studied by nanodiffraction. Rapid and detailed diffraction maps were recorded by scanning the position of the sample using the piezoelectric positioner while recording the intensity of the Au (222) Bragg reflection. The scanning required acquisition times of the order of 1 s for each point in the raster scan from which the image was formed, with minimal mechanical settling time between subsequent points. Scanning diffraction microscopy images with both large (30 μm × 20 μm) and small (several μm) fields of view before and after the 30 min annealing step are shown in Figure 7. The same general distribution of islands landscape is found within this area, with a shift of the sample position by approximately 3 μm during the thermal cycle. The streaking of Au the
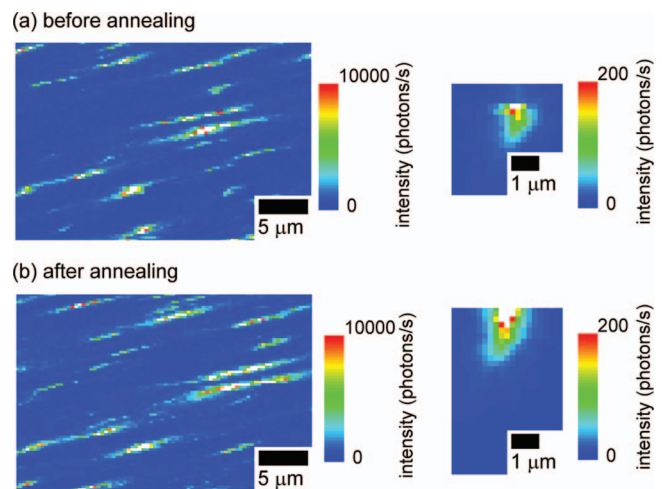

FIG. 7. X-ray diffraction nanodiffraction images of the intensity of the Au (222) reflection acquired (a) immediately after the initial formation of Au (111) islands from the Au/Si eutectic, but before subsequent annealing, and (b) after the annealing step. Smaller scale images (at right) illustrate the sample motion resulting from the annealing cycle, approximately 3 μm in the vertical direction.
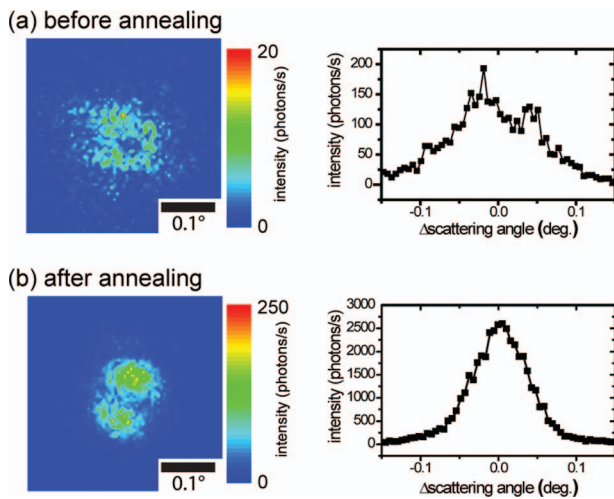
FIG. 8. X-ray diffraction patterns for the Au (222) reflection acquired (a) after Au (111) island formation from the Au/Si eutectic liquid, but before annealing, and (b) after annealing. Annealing results in a sharpening of the diffraction peak and an increase in peak intensity by a factor of 17. These changes are consistent with a significant increase in the size of the crystals and a decrease in their degree of misorientation with respect to the sample surface normal, and the concentration of extended defects.

mapping features associated with Au islands occurs because the images were acquired before waiting for thermal transients to decay.

The utility of a rapid scanning procedure becomes evident in such annealing experiments because faster scanning reduces the effects arising from thermal drift of the sample and sample holder. Rapid maps are possible because the sample environment has sufficiently low mass that it can be translated by the piezoelectric positioners. The shift in the sample position is more visible on the spatial diffraction mapping recorded only on one particular island, shown in the small scale maps of Figures 7(a) and 7(b) before and after annealing. Thermal hysteresis as the temperature is cycled between the measurement and annealing temperatures results in an apparent shift of the position of the island by 2.8 μm. This can be taken as an estimate of the long-term position stability of the sample holder.

Figure 8 shows diffraction patterns acquired from the island that appears in the smaller range maps of Figure 7. A comparison of the diffraction peaks in the two cases shows that the annealing step results in a sharpening of the Au (222) reflection. The full width at half maximum (FWHM) of the (222) Bragg reflections are similar, and mainly dominated by the beam divergence, but the maximum intensity is more than 10 times higher in the annealed state. The second heating step thus further establishes the preferred (111) orientation of the Au islands.

IV. CONCLUSION

Lightweight UHV sample environments for x-ray nanodiffraction studies allow nanobeam x-ray experiments under a range of temperatures of interest for the study of *in situ* processes in materials. The specific case of the dewetting of an Au thin film demonstrates that nanobeam diffraction, reflectivity, and scanning diffraction microscopy can be applied using a small UHV chamber designed for high stability and positioning precision. The strategy of using small mechanically decoupled UHV sample environments opens new ways to study nanoscale materials using nanodiffraction combined with *in situ* heating in vacuum or in controlled gas environments.

[1] G. E. Ice, J. D. Budai, and J. W. L. Pang, Science **334**, 1234 (2011).
[2] P. G. Evans and S. J. L. Billinge, MRS Bull. **35**, 495 (2010).
[3] T. U. Schulli, R. Daudin, G. Renaud, A. Vaysset, O. Geaymond, and A. Pasturel, Nature (London) **464**, 1174 (2010).
[4] V. L. R. Jacques, D. Le Bolloc'h, S. Ravy, J. Dumas, C. V. Colin, and C. Mazzoli, Phys. Rev. B **85**, 035113 (2012).
[5] J. Y. Jo, P. Chen, R. J. Sichel, S.-H. Baek, R. T. Smith, N. Balke, S. V. Kalinin, M. V. Holt, J. Maser, K. Evans-Lutterodt, Chang-Beom Eom, and Paul G. Evans, Nano Lett. **11**, 3080 (2011).
[6] E. Mannebach, J. W. Spalenka, P. S. Johnson, Z. Cai, F. J. Himpsel, and P. G. Evans, Adv. Funct. Mater. **23**, 554 (2013).
[7] V. L. R. Jacques, D. Carbone, R. Ghisleni, and L. Thilly, Phys. Rev. Lett. **111**, 065503 (2013).
[8] P. G. Evans, E. D. Isaacs, G. Aeppli, Z. Cai, and B. Lai, Science **295**, 1042 (2002).
[9] R. P. Winarski, M. V. Holt, V. Rose, P. Fuesz, D. Carbaugh, C. Benson, D. Shu, D. Kline, G. B. Stephenson, I. McNulty, and J. Maser, J. Synchrotron Radiat. **19**, 1056 (2012).
[10] Y. Suzuki, A. Takeuchi, H. Takano, and H. Takenaka, Jpn. J. Appl. Phys., Part 1 **44**, 1994 (2005).
[11] H. Mimura, H. Yumoto, S. Matsuyama, Y. Sano, K. Yamamura, Y. Mori, M. Yabashi, K. Nishino, K. Tamasaku, T. Ishikawa, and K. Yamauchi, Appl. Phys. Lett. **90**, 051903 (2007).
[12] B. Lai, W. B. Yun, D. Legnini, Y. Xiao, J. Chrzas, P. J. Viccaro, V. White, S. Bajikar, D. Denton, F. Cerrina, E. Difabrizio, M. Gentili, L. Grella, and M. Baciocchi, Appl. Phys. Lett. **61**, 1877 (1992).
[13] B. Lengeler, C. G. Schroer, M. Richwin, J. Tummler, M. Drakopoulos, A. Sinigirev, and I. Snigireva, Appl. Phys. Lett. **74**, 3924 (1999).
[14] B. Gorges, H. Vitoux, P. Redondo, G. Carbone, C. Mocouta, and G. Guilera, AIP Conf. Proc. **1234**, 572 (2010).
[15] F. Bertram, C. Deiter, K. Pflaum, and O. H. Seeck, Rev. Sci. Instrum. **83**, 083904 (2012).
[16] K. Jefimovs, O. Bunk, F. Pfeiffer, D. Grolimund, J. F. van der Veen, and C. David, Microelectron. Eng. **84**, 1467 (2007).
[17] C. Ponchut, J. M. Rigal, J. Clément, E. Papillon, A. Homs, and S. Petitedemange, J. Instrum. **6**, C01069 (2011).
[18] E. Jiran and C. V. Thompson, J. Electron. Mater. **19**, 1153 (1990).
[19] E. Jiran and C. V. Thompson, Thin Solid Films **208**, 23 (1992).